Received: 14 July 2022 | Revised: 20 October 2022 | Accepted: 19 November 2022

DOI: 10.1002/jemt.24269

RESEARCH ARTICLE

MICROSCOPY RESEARCH & TECHNIQUE WILEY

Histological, elemental, and ultrastructural analysis of melanin in mantle of Pacific oyster (*Crassostrea gigas*)

Zhuanzhuan Li[1] | Qi Li[1,2] | Chengxun Xu[1] | Hong Yu[1]

[1]Key Laboratory of Mariculture, Ministry of Education, Ocean University of China, Qingdao, China

[2]Laboratory for Marine Fisheries Science and Food Production Processes, Qingdao National Laboratory for Marine Science and Technology, Qingdao, China

Correspondence
Qi Li, Key Laboratory of Mariculture, Ministry of Education, Ocean University of China, Qingdao, China.
Email: qili66@ouc.edu.cn

Funding information
National Nature Science Foundation of China, Grant/Award Number: 31972789; China Agriculture Research System Project, Grant/Award Number: CARS-49; The Earmarked Fund for Agriculture Seed Improvement Project of Shandong Province, Grant/Award Numbers: 2020LZGC016, 2021LZGC027

Review Editor: Alberto Diaspro

Abstract

Colorful shell of bivalve is mainly because of the biological pigments, of which melanin plays an important role in shell color formation. More and more studies focus on the genes function involved in melanin synthesis, but relatively few studies address the biochemical character and ultrastructure of melanin in bivalve from microscopic perspective. Here, we investigated the histological structure of mantle of *Crassostrea gigas* with orange shell color. Distribution of melanin in mantle was verified with histochemical staining. In addition, immunofluorescence technique showed that strongly positive signal of CgTYR was specific to the mantle margin, which is consistence with the location of brown granules in H&E staining. The further result of elementary composition of melanin displayed that metal Ca, Fe, and Zn were detected using scanning transmission electron microscope and energy dispersive spectroscopy mapping methods. Next, based on TEM observations, it was speculated that the series of cellular events leading to the formation and release of melanin. Melanocyte in the primary stage showed many mitochondria and rough endoplasmic reticulum as well as an extensive Golgi complex with numerous vesicles intermingled with melanosome. Subsequently, melanosome was expended and their hue gradually intensified, and Golgi complex and mitochondria were still observed in the cytoplasm. Finally, after melanosome was discharged into intercellular spaces, the disintegration of membranes in some cells, and severe cellular vacuolization. These data enrich the understanding of ultrastructural characteristic and formation of melanin in mantle of bivalve and pave the way for further investigating shell coloration at the cellular level.

KEYWORDS

Crassostrea gigas, immunofluorescence, melanin, scanning transmission electron microscope energy dispersive spectroscopy mapping, transmission electron microscopy

Research highlights

1. Melanocytes were observed in mantle *of C. gigas* using TEM.
2. Elemental distribution of melanosome in mantle of *C. gigas* was detected using STEM EDS mapping method for the first time.
3. The supposed melanogenesis in mantle of *C. gigas* was analyzed.

1 | INTRODUCTION

The shells of mollusks are unique example of complex patterns during the ontogenesis, in which the whole developmental processes are recorded. Usually, shell biomineralization is achieved by the underlying mantle, a thin sheet of tissue that overlies the dorsal surface of mollusks, it can secrete proteins and other components that form the shell's organic matrix (Addadi et al., 2006). Furthermore, shell color formation is also own to the pigmentation at the edge of the mantle (Brake et al., 2004). Melanin is the most common pigment that closely related to the shell color (Saenko & Schilthuizen, 2021). To date, more and more studies revealed that genes related to melanin synthesis have vital roles in shell color in bivalves (Feng et al., 2019; Lemer et al., 2015; Li et al., 2021, 2022; Min et al., 2022; Palumbo, 2003; Yu et al., 2018, 2018b; Zhang et al., 2018; Zhu et al., 2021). However, it was neglected that the biochemical characters, distribution and melanogenesis studies of melanin in mantle of bivalve.

Melanin has attracted considerable interest because of their involvement in pigmentation and protection against ultraviolet, metal binding and many other unique properties (Ito et al., 2013). Metal chelation is an important biological function of melanin. Using energy dispersive spectroscopy (EDS) technical detection, more studies have revealed that melanin in vertebrate contained metal element, like Ca, Fe, Zn, and Cu (Biesemeier et al., 2011, 2016; Eibl et al., 2006; Hong et al., 2004; Liu & Simon, 2005; Madkhali et al., 2019). Nevertheless, relatively little information about metal composition of melanin has been obtained in bivalve compared to vertebrates. Besides, visualization of melanin is brown with hematoxylin and eosin (H&E) staining, which is nonspecific for melanin when the pigment is scarce or other pigments are present. In view of this, other histochemical techniques are also used for melanin identification, such as the ferrous sulfate technique, potassium permanganate bleaching, and the Masson-Fontana method (Carriel et al., 2011; Żądło & Sarna, 2019). Shataer et al. (2020) and Zhang et al. (2020) considered that the ferrous sulfate method was more suitable for special staining of melanin than other methods. At molecular level, melanin synthesis is related to the expression of melanocytes differentiation and migration related proteins, such as tyrosinase gene family, including tyrosinase (Tyr), tyrosinase-related protein 1 (Tyrp1), and tyrosinase-related protein 2 (Tyrp2) (Fang et al., 2001; Hartman & Czyz, 2015). In vertebrate, a large number of melanocytic markers have been investigated, among of these, TYR is a highly specific and sensitive marker for melanocytic differentiation (Ordóñez, 2014; Saliba & Bhawan, 2021). Nevertheless, to our knowledge, rare paper related to immunohistochemical makers of melanin in bivalve was published, because in previous studied cases, melanin granule was commonly identified using histochemistry staining (Bravo Portela et al., 2012; Han et al., 2022; Jiang et al., 2020; Martin et al., 2021; Nogal & García, 2015).

In vertebrate, melanin is located almost exclusively within well-defined submicron melanosome, specialized organelles derived from early endosomal membranes whose functions are to synthesize and store melanin. And the formation process of melanosomes is well studied that need a series of well-defined stages (D'Alba & Shawkey, 2019). In contrast, current models of molluscan melanosomes are heavily based on observations from cephalopods (Jiang et al., 2020; Palumbo, 2003). There are significant structural and genetic differences between different molluscan classes (Jackson et al., 2010). Now, as far as we know, only a few reports identified the distribution and ultrastructure of melanin in the mantle of Pacific oyster (*Crassostrea gigas*) using three melanin staining method or transmission electron microscopy (TEM) methods (Han et al., 2022). Hence, it is necessary to focus on the more details in ultrastructure of melanin and melanogenesis in bivalve.

In the present study, the mantle tissue in *C. gigas* with orange shell color was studied. Melanin in mantle was identified base on histochemistry staining and immunofluorescence (IF) methods. The ultrastructure of melanin and melanogenesis in mantle was also investigated by means of TEM. Besides, elemental analysis of melanosome was examined by scanning transmission electron microscope (STEM) EDS mapping technology for the first time. Taken together, this study presented ultrastructural findings on melanin in mantle of *C. gigas* in order to characterize the cells that are responsible for melanin formation.

2 | MATERIALS AND METHODS

2.1 | Animals

Several adults of Pacific oysters with orange shell color were collected from Rongcheng, Shandong province, China. The oysters were cultivated with the recirculating seawater at 23–25°C for 10 days in laboratory before sampling. Prior to the following experiment, five healthy oysters (shell length: 48 ± 5.88 cm; shell height: 82.15 ± 8.26 cm) were dissected to obtain mantle samples used for light microscopy (LM), IF, and TEM examinations. The Pacific oyster is neither an endangered nor protected species. All experiments in this study were conducted according to national and institutional guidelines.

2.2 | Light microscopy

Histological examinations of tissues were based on the methods described by Ruska et al. (2020) with some modifications. All samples were fixed directly with Bouin' solution (Sbjbio life Science, Nanjing) for 24 h, dehydrated using gradient ethanol (75%, 80%, 90%, 95%, and 100%) for 30 min each time, vitrified for 5 min by dimethylbenzene and embedded in paraffin wax. The paraffin wax tissue blocks were processed for sectioning at a thickness of 5 μm using a semiautomated rotatory microtome. Then the paraffin sections obtained were collected on glass slides, cleaned in xylene, and dehydrated by immersing in serial dilutions of ethyl alcohol-water mixture. Afterward, the slices were stained with H&E dye in preparation for histological examinations under an Olympus BX53 light microscope (Olympus Corporation, Japan).

Ferrous sulfate staining was performed with ferrous sulfate staining kit (Leagene, DJ002, China) according to the manufacturer's instructions. Simply, after dewaxing, the sections were immersed in ferrous sulfate solution for 45 min and washed with ultrapure water for 5 min three times. Then the samples were placed in acid potassium ferricyanide solution (potassium ferricyanide: 4% ethanoic acid: ultrapure water = 2:1:1) for 30 min and then were differentiated in acetic acid for 20 s. Finally, the samples were counterstained with nuclear fast red solution for 2 min. After washing, the tissue samples were viewed under an Olympus BX53 light microscope (Olympus Corporation, Japan).

2.3 | Immunofluorescence

Additional serial sections (5 μm thickness) mounted on poly-lysine-coated slides were used for immunohistochemical investigations. The sections were cleaned in xylene and dehydrated by immersing in gradient ethyl alcohol (100%, 95%, 80%, and 70%). Then, sections were washed in PBS for 5 min twice. Next, antigen retrieval was performed in 0.01 M citrate buffer (pH 6) at 100°C for 10 min and then cooled naturally to the room temperature. Prior to reacting with primary antibody, sections were blocked with 7.5% goat serum (Beyotime) at room temperature for 30 min. After blocking nonspecific binding cites, antibody incubation was performed with rabbit polyclonal anti-CgTYR primary antibody (antibodies obtained from our previous study that not published, 1:50 dilution) at 37°C for 1 h and subsequently at 4°C overnight. Sections were then incubated with Alexa fluor® 488-labbled Goat Anti-Rabbit secondary antibody (1:500 dilution, cat. nos. A0423, Beyotime) at room temperature for 1 h. The negative controls were incubated with normal goat serum. Cell nuclei were counterstained with DAPI (Beyotime) for 5 min at room temperature. Finally, samples were mounted onto glass slides and images were captured using confocal microscopy (TCS SP98, Leica, Germany) and examined by LASX software (Lecia).

2.4 | Transmission electron microscopy

Mantle tissue isolation for the ultrastructure analysis was performed according to Jiang et al., 2020. Briefly, the isolated mantle with 1 mm^3 was fixed in 2.5% glutaraldehyde at 4°C. Specimens were postfixed with 1% osmic acid for 2 h and washed in 0.1 M phosphate buffer (pH 7.0) for 10 min three times, dehydrated by immersing in serial dilutions of ethanol (30%, 50%, 70%, 90%, and 100%) for 10 min each time, and then embedded in EPON 812 resin at room temperature and solidified in 37, 45, and 65°C for 24 h each time. Finally, ultrathin sections (60 nm) obtained were stained with uranyl acetate for 15 min, following with lead citrate for 15 min and then examined under a JME-1200EX transmission electron microscope (JEOL, Japan) operated at 80.0 kV. In addition, other unstained sections (60 nm) were used for the next analysis.

2.5 | STEM EDS mapping analysis

For elemental analysis of melanin, the unstained ultrathin sections (60 nm) were mounted on Ni grids. STEM EDS mapping analysis were performed on a Zeiss sigma 500 SEM, and an EDS detector (Oxford X-Man 80) operated at 20.0 kV with a magnification of 15,000 X. The spectra were collected with activity time of 10 min. The chemical composition of the melanin was analyzed using EDS spectroscopy. The EDS spectra was quantitatively analyzed by the INCA software

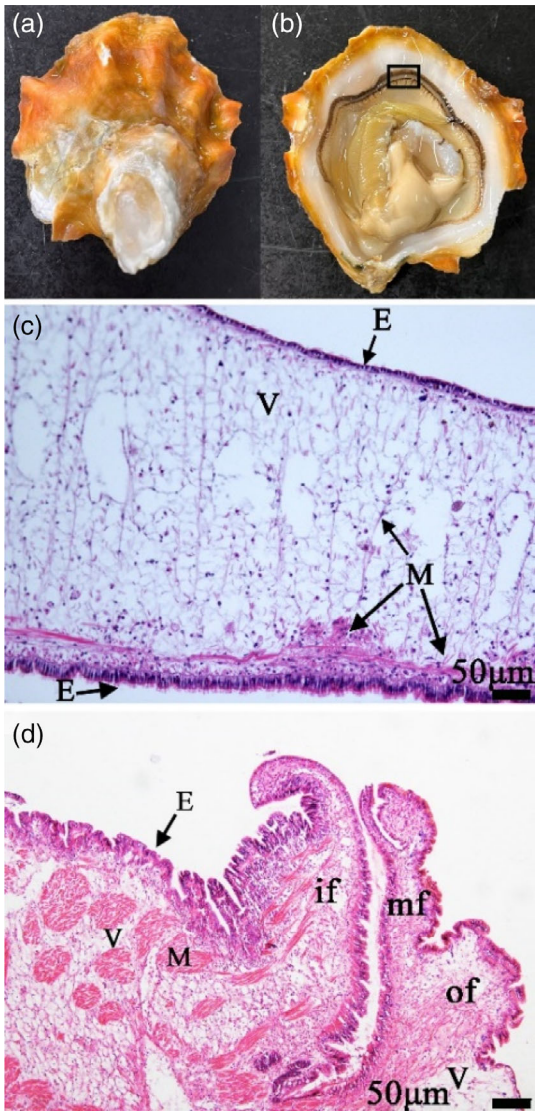

FIGURE 1 H&E staining of mantle in *C. gigas*. (a) The right shell of oysters with orange shell color. (b) The area of mantle tissues used for paraffin section analysis. (c) Central zone of mantle in *C. gigas*. The epithelia (e) enclose loosely packed interstitial tissue containing muscle (M), vesicular cell (V). Thin bands of muscles (M) traverse the mantle and lie against the epithelial layer. (d) the tissue is more densely packed than in the central zone. The mantle margin formed into three major folds: Outer fold (of), middle fold (mf), and inner fold (if)

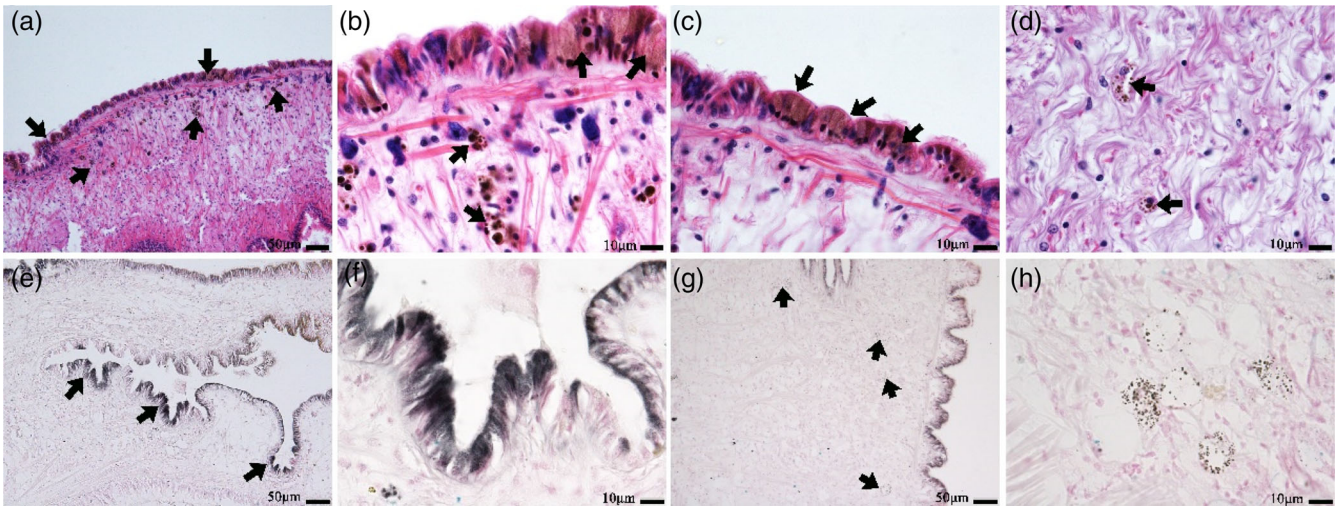

FIGURE 2 Light microscopy observation about melanin granules in mantle of *C. gigas*. (a–d) Melanin granules in mantle with H&E staining. (a, b) Melanin granules were stained brown (black arrows). (c) Brown granules with no limiting membrane lie in the cytoplasm of epithelium. (d) Brown granules were coated with membrane in connected tissue. Scale bar is 50 μm in (a), scale bars are 10 μm in (b), (c) and (d). (e–g) melanin granules in mantle with ferrous sulfate staining. Melanin granules reacted dark green or black with ferrous sulfate (black arrows). Scale bars are 50 μm in (e) and (g), scale bars are 10 μm in (f) and (h)

(INCA 2001) using the standardless Cliff-Lorimer-k-factor method. The k factors were those used in Eibl et al. (2006).

3 | RESULTS

3.1 | Histology of mantle in *C. gigas*

The right shell of oyster with orange shell color and the area of mantle tissues used for histology analysis was shown in Figure 1a,b, respectively. The mantle of oyster can be divided into the central zone and the edge of the mantle, the former consists of a sheet of tissue with thin epithelia (E) separated by a loose interstitial tissue containing muscles (M) and variable numbers of large vesicular cells (V) (Figure 1c). There were generally loosely packed vesicular cells and large extracellular spaces, often traversed by thin muscle fibers (Figure 1c). Near the mantle margin, the tissue became more densely packed with muscles (M), vesicular cells (V) and collagen fibers, and the extracellular spaces were smaller (Figure 1d). The edge of the mantle was crossed by several bands of dense muscles (M). Muscles fibers ran across from the base of the inner fold to the base of the outer fold. Between the muscle bands, there were clusters of vesicular cells (V) and usually several clumps of calcified granules. And the typical three folds, outer fold (of), middle fold (mf), and inner fold (if) were observed in the mantle margin.

3.2 | LM observation of melanin in mantle of *C. gigas*

A cluster of spherical or irregular brown-staining pigment granules were present in the mantle margin epithelium and connective tissue after H&E staining (Figure 2a–d). In epithelium, numerous brown granules with no limiting membrane lie in the cytoplasm (arrowhead in Figure 2c), whereas in connective tissue, there were a thin film enclosed a lump of brown granules (arrowhead in Figure 2b,d). The nature of the melanin is that it can react with ferrous iron. To investigate whether granules were melanin further, ferrous sulfate method was performed to explore histological staining changes. Along the mantle epithelium quite abundant granules are stained dark green or black with ferrous sulfate (arrowhead in Figure 2e,f), which was the same with the result of that in connective tissue (Figure 2g,h).

In addition, immunofluorescence with CgTYR was used to detect melanin in mantle. The positive CgTYR signals existed mainly in cytoplasm of epithelium in mantle margins (Figure 3, b1–b3), which was in keeping with the result of H&E staining (Figure 3, a1–a3). The distribution and immune-fluorescence intensity of CgTYR exhibited the existence of melanin in mantle of *C. gigas*.

3.3 | TEM observation of melanosome in mantle of *C. gigas*

Using TEM, the side epithelial cells were typically columnar in edge of the mantle margin (Figure 4a). And epithelial secretory cells were scattered among epithelial cells, they were similar in shape and appearance to goblet cells, and characterized by an apical surface swollen with secretory granules and a narrow basal region (Figure 4a,b,d). The secretory granules of the cells identify here as type "A" are completely electron-lucent, very tightly packed and occupy the entire cytoplasm. Moreover, the mantle contained varying quantities of homogeneous and electron dense granules, melanin granules (mg) (200–600 nm diameter) (Table S1), usually existed in microvillar cells of epithelial tissues (Figure 4a–c) and connected tissues

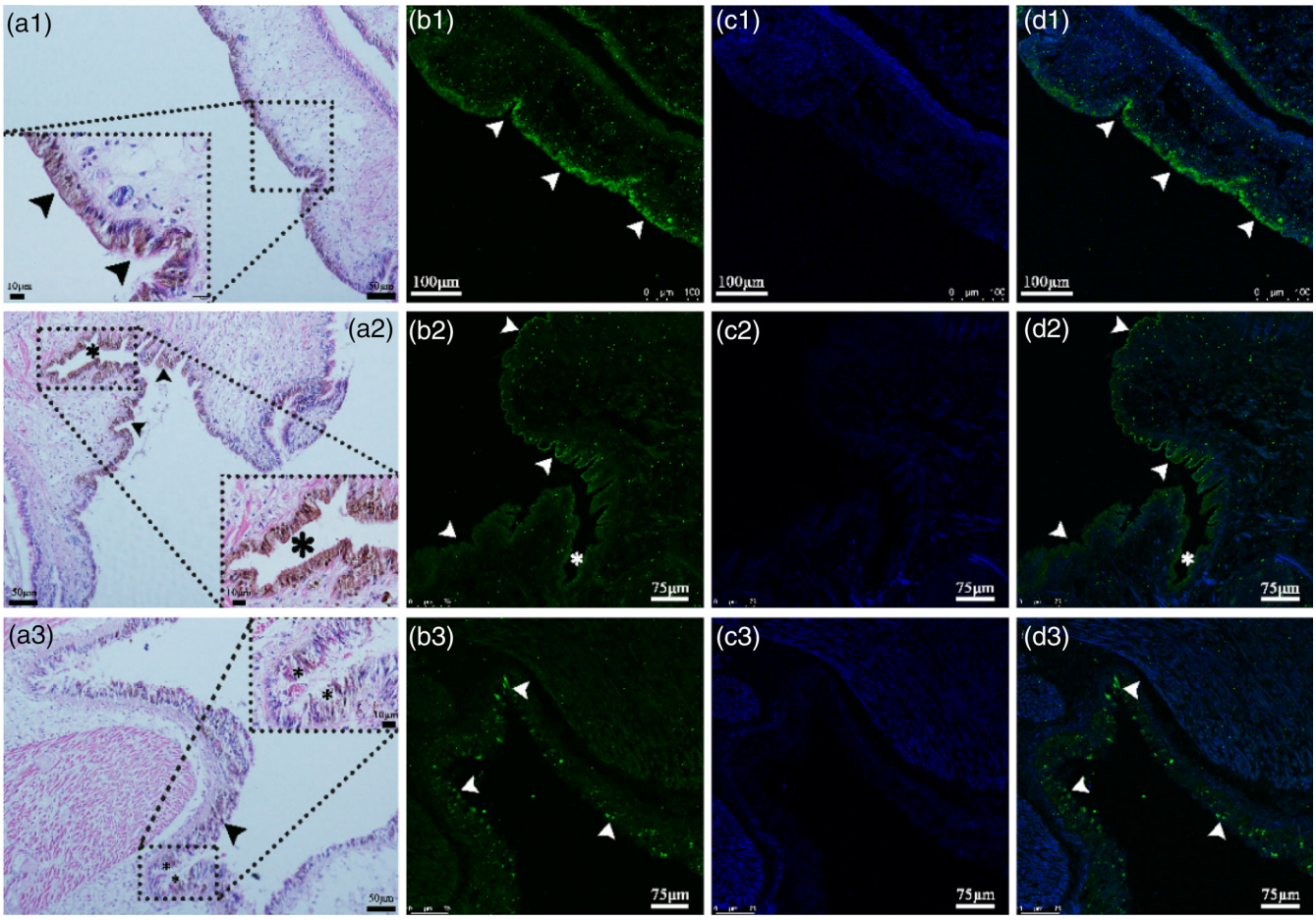

FIGURE 3 Fluorescence microscopy images on melanin granules labeled with CgTYR antibody. Immunohistochemical results showed that the staining of CgTYR in the mantle margins (white arrows in b1–b3). The fluorescence signals (white arrows in b1–b3) were consistent with the melanin granules in H&E staining (black arrows in a1–a3). Nuclei was stained using DAPI in c1–c3. d1–d3 shown the merge results of b1–b3 and c1–c3, respectively

(Figure 4d–f). A numerous round, electron-dense pigment granules covered by a vesicle are scattered among the epithelial cells (Figure 4c). In connected tissues, many homogeneous and electron dense granules with limiting membrane lie in the cytoplasm of melanocyte, which has completed cellular structure including nuclei, mitochondria, and Golgi complex in cytoplasm (Figure 4g–i). In addition, Golgi complex and mitochondria are mainly distributed around the melanin granules, particularly associated with the melanin granules formation.

3.4 | STEM EDS mapping analysis of melanosome in mantle of *C. gigas*

Elemental composition of melanin granules in mantle of *C. gigas* were analyzed using STEM EDS mapping method. Figure 5 (a1 and a2) showed TEM images of a typical area of melanosome, nuclei, mitochondria, endoplasmic reticulum and Golgi complex, enclosed in melanocyte in two different area of connective tissues in the mantle. EDS spectrum of melanin granules was investigated. EDS microanalysis of melanosome yielded mole fractions for metallic element Ca, Fe, and Zn, other elements also observed, like, N, O, P, S, and Cl (Figure 5, b1 and b2). Os-K α peaks originates from the stray radiation of the sample fixed in osmic acid. Qualitatively, the spectra of all melanin granules in Figure 5 (a1 and a2) look similar. Relevant elemental maps were shown in Figure 5 (c1 and c2). Element O, N, P, S and metallic element like Ca, Fe, and Zn locations was kept the consistency of the location of melanin granules in Figure 5, (a1) and (a2), respectively.

3.5 | The supposed melanogenesis in mantle of *C. gigas*

In connected tissues, deeply pigmented melanin cells were stained brown granules after H&E staining (Figure 2a–d). Ultrastructure examination revealed that deeply melanocyte containing a large number of cytoplasmic melanosomes were found (Figure 6a). Exactly, it could be distinguished two different melanocytes (denoted as M1 and M2) which contained two different electron-dense components and may correspond to different stages of melanosome development

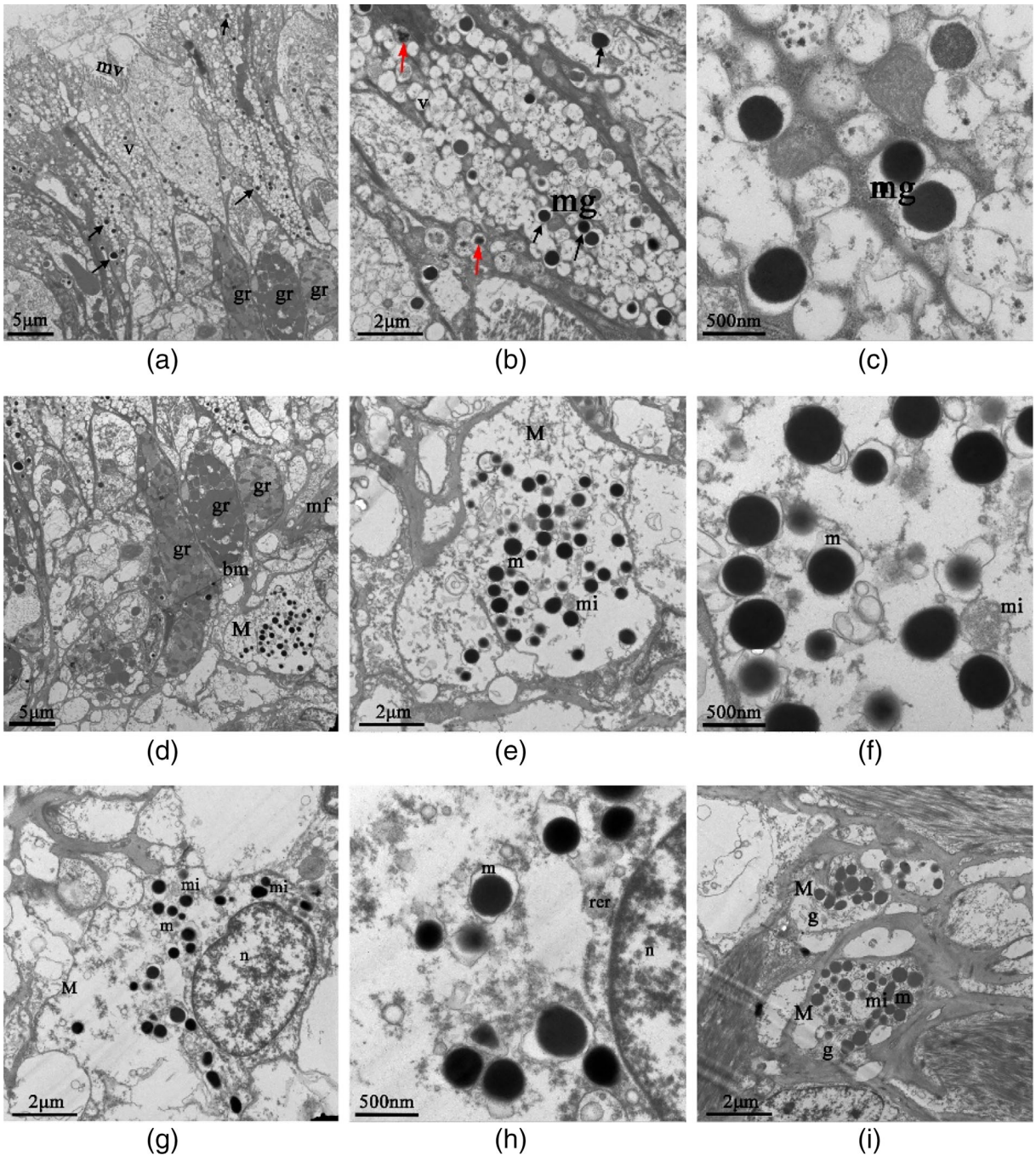

FIGURE 4 Transmission electron microphotographs of melanosome in mantle of *C. gigas*. (a) General view showing secretory cells and pigmented epithelial cells with a prominent microvillus border (mv). Vesicles (v), granules (gr) and melanin granules (mg; as shown by black arrows). (b, c) Details of melanin granules (black arrows) and partially melanized granules (red arrows) in epithelial cells. (d) General view showing the melanocytes (M) filling with melanin granules in connective tissues, in which muscle fiber (mf) were observed. Melanocytes (M) were sited in connective tissues and next to the base member (bm). (e, f) Details of melanocyte. Several melanosomes (m) and mitochondria (mi) were observed in melanocyte. (g–i) Details of melanocyte (M) in connective tissues. Melanosomes (m), mitochondria (mi), rough endoplasmic reticulum (rer), Golgi complex (g) and nucleus (n) were detected in melanocytes

(Figure 6a). Melanocytes in the primary stage (M1) showed many mitochondria and rough endoplasmic reticulum (rer) as well as an extensive Golgi complex with numerous vesicles intermingled with melanosomes (Figure 6b,c). Moreover, except rounded melanosomes, other melanosomes were small and light-black granules, in which, there were many partially melanized organelles that contained two different electron-dense components and may correspond to an early stage of melanosome development (Figure 6c). Subsequently, the melanosomes developed further and the granules were expended as well as their color gradually intensified, electron-dense melanosomes

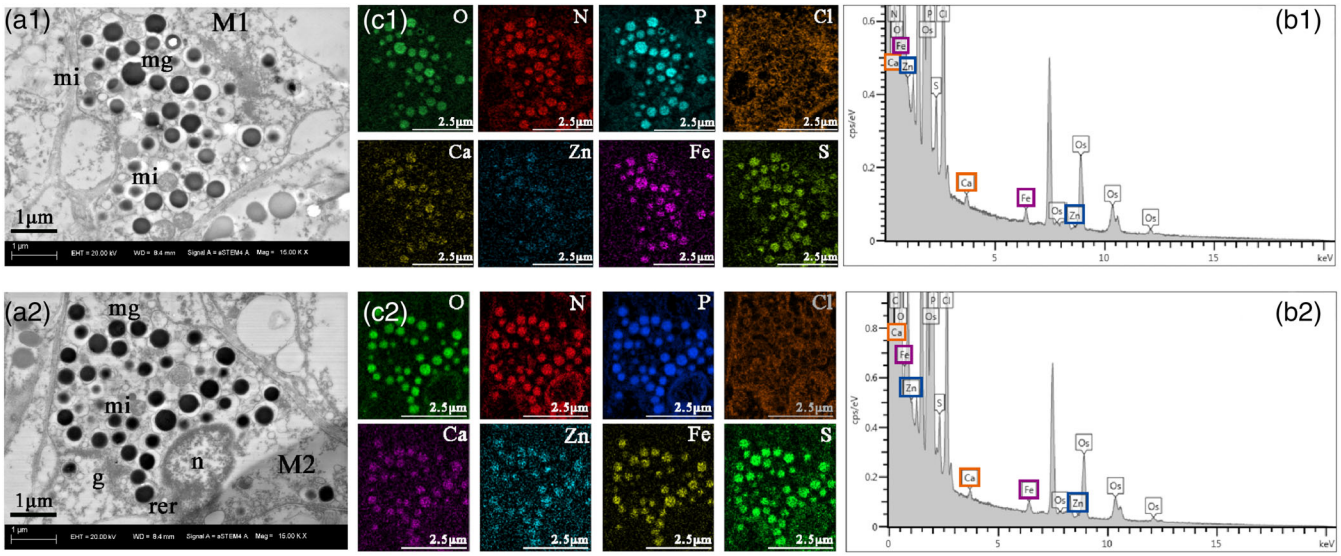

FIGURE 5 EDS spectra analysis and elemental maps of melanosome in mantle of *C. gigas*. (a1, a2) TEM of melanosome from two different developmental melanocytes in connective tissues. Mitochondria (mi), rough endoplasmic reticulum (rer), Golgi complex (g), nucleus (n) were detected in melanocytes. (b1, b2) EDS spectra of melanosomes. Signals acquisition area of EDS spectra of melanosome in melanocytes from Figure 5 (a1), (a2), respectively. Note the metallic element Ca and trace element like Fe and Zn were detected (colorfult box). Artifact peaks are Os from the sample fixed in the osmic acid. (c1, c2) elemental analysis of melanosomes in melanocytes from Figure 5 (a1), (a2), respectively. Elemental compositions map of melanosomes was obtained using STEM EDS mapping method. Element O, N, P, S and metallic element like Ca, Fe, and Zn locations was kept the consistency of the location of melanosome in melanocytes, respectively

getting darker. Besides, Golgi complex and mitochondria were also observed in cytoplasm of melanocytes (M2) (Figure 6d,e). Finally, after melanosomes were discharged into intercellular spaces, the disintegration of membranes in some cells, and severe cellular vacuolization (Figure 6f). Furthermore, expect for nuclei was no obvious effects, organelles such as mitochondria, Golgi complex, and endoplasmic reticulum, were dissociated and damaged.

4 | DISCUSSION

In this study, the biochemical and ultrastructural features of melanin in mantle of Pacific oyster was systematically described. From a morphological perspective, the organization structure of the mantle edge is very similar in the *Velesunio ambiguous* (Colville & LimA, 2003) and *Haliotis asinine* (McDougall et al., 2011), which was thickened and formed into three major folds: outer fold that are required for secretion, and middle fold that plays a role in sensation and inner fold acting in muscle. Because the periostracum emerged from the groove between the outer and middle folds, the out fold was further divided into two or more lobes (Colville & LimA, 2003). However, with minor differences in the appearance of the number of middle grooves in *C. gigas* and other species. The outer mantle epithelium is responsible for secretion of the inner layers of the shell (Istin & Masoni, 1973). The outer epithelial cells in *C. gigas* are similar in structure to the outer epidermal cells in Pteriidae (*Pinctada radiata* (Pteriidae) and *Isognomo alatus* (Isognomonidae)) and Haliotidae (*H. tuberculata*) (Nogal & García, 2015), containing numerous mitochondria and endoplasmic reticulum cisternae *Anodonta* (Bubel, 1973; Machado et al., 1988), which was cellular machinery to suggest secretion of shell material. Inversely, in *Anodonta* species, the outer epithelial cell appears to function mainly to store glycogen and there was little cellular machinery to suggest secretion of shell material. This difference in cellular structure may reflect phylogenetic difference or functional differences.

A cluster of spherical or irregular brown-staining pigment granules were present in the mantle margin epithelium and connective tissue after H&E staining (Figure 2a–d). Related study shown that these brown particles were melanin in *Sepia pharaonis* (Jiang et al., 2020). In addition, histochemical reaction was used to detect melanin that it can turn dark-green or black with ferrous iron (Jabbour-Zahab et al., 1992). In this study, the ferrous iron technique used showed positive reaction, indicating the granules were melanin. According to our immunofluorescence results, TYR signal was consistently observed in mantle margins of *C. gigas*. CgTYR is very useful and highly specific for the melanin in many Melanomas' research (Ordóñez, 2014; Saliba & Bhawan, 2021; Xu et al., 2002). Here, the immunofluorescence data of TYR also shown that CgTYR was a specific maker for melanin in mantle of *C. gigas*.

The epidermal cells of mantle are associated with pigmentation of the shell in bivalve. In order to better understand the roles of melanin in shell color formation, we addressed ultrastructural and elemental study of melanin. TEM observation showed that mantle epithelium cells was highly pigmented with melanin granules and possessed a prominent microvillus border. The similar cases of melanin in epithelium have been described in mantle

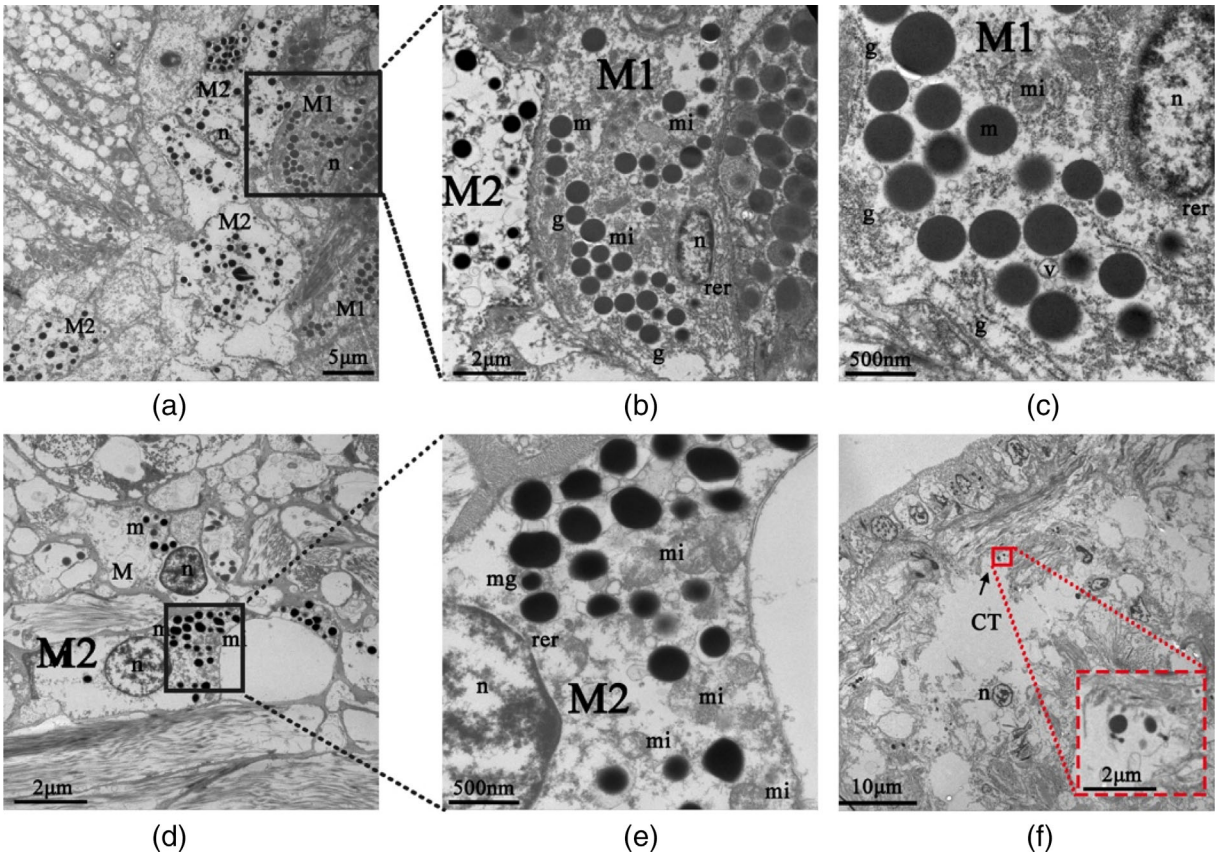

FIGURE 6 The developmental process and release of melanin in mantle of *C. gigas*. (a) Different developmental stages of melanocytes (M) (M1 and M2) were shown depending on the different electron densities melanin granules. In M1, melanosomes were shallow and the cytoplasm filling full with the organelle, which is related to the producing of melanin granules. In M2, melanosomes were dark and the organelle in cytoplasm became less maybe related to the mature of melanin granules. Bar in (a) is 5 μm. (b-c) Abundant mitochondria (mi), rough endoplasmic reticulum (rer) and Golgi complex (g) with numerous vesicles (v) intermingled with the melanosomes in melanocytes. Bar in (b) is 2 μm. Bar in (c) is 500 nm. (d-e) Melanosomes were further developed larger and darker in M2. Bar in (d) is 2 μm. Bar in (e) is 500 nm. (f) the ultrastructure of the melanocyte under melanin release. The membrane of melanocyte was disintegrated and cell was vacuolated. The melanin was released by exocytosis (as shown in red box). Bar in (f) is 10 μm. Bar in red box in (f) is 2 μm

epithelium of Gastropoda, *H. tuberculata* (Nogal & García, 2015) and the side foot of *H. tuberculata* (Bravo Portela et al., 2012). Melanocytes contained mature and nonmature melanosomes, the same finding was also observed in epithelium of *S. officinalis* (Jiang et al., 2020; Schraermeyer, 1994). However, unlike the above, the similar pigmented cells were provided a red-purple color to the skin of *Aplysia californica* (Prince & Young, 2010), no melanin granules were described. What the specific substance needs to be further studied. It was reported that the pigment is in the form of membrane-bound vesicles or melanosome (Jiang et al., 2020). Overall, TEM observations revealed that histological morphology of melanosome or melanocyte in mantle of *C. gigas* was like that observed in foot epithelium of the ablone *H. tuberculate* (Bravo Portela et al., 2012) and skin epithelium of keyhole limpet *Megathura crenulate* (Martin et al., 2021). Additionally, another structure of melanin was observed in the epithelium of mantle in *H. tuberculate* that melanin was arranged as spiral membranes (Nogal & García, 2015). Similar structures have been described in the epithelium of the cephalic tentacles of *Diodora* sp. (Künz & Haszprunar, 2001), however, they were described as secretory granules belonging to mucous cells.

The elemental analysis was carried out to uncover the characters of melanosome in mantle of *C. gigas*, the result displayed that melanosome composed of N, O, P, S, Cl and metallic element Ca, Fe, and Zn. Similarly, melanosome in retinal tissues of human, monkey, and rat were also analyzed by EDX in the TEM, among of these, mole fraction of transition metals Fe, Ca, Cu, and Zn was also measured (Eibl et al., 2006). And it was outlined that the similar and differences between the different species. Nature melanin have properties to dope with various transition metals (Fe, Cu, and Zn ions) (Madkhali et al., 2019). Iron adsorption has also been reported in Sepia melanin (Liu & Simon, 2003) and some researchers have investigated the binding capacity of Sepia melanin to Mg, Zn, Fe, and Cu (Liu & Simon, 2005; Sarzanini et al., 1992). Metal chelation is one of the most important biological functions of melanin. Here, the present study was corresponding to the previous reports, it was speculated that melanosome in mantle of *C. gigas* maybe also have the biological function in chelating mental.

Our TEM observations showed that melanocyte in mantle of *C. gigas* was similar with the type B cell in ink gland of squids (Jiang et al., 2020) and octopuses (Wang et al., 2011). Type B cells were mainly composed of cell membrane, melanosomes, vesicles, mitochondria, Golgi apparatus, endoplasmic reticulum, and nuclei, which are the sites of melanin synthesis and secretion (Palumbo, 2003). Based on TEM observation, it was found that melanogenesis in *C. gigas* was similar with the general melanogenesis pathway in vertebrates (Schraermeyer, 1994). At the beginning, the rough endoplasmic reticulum contains active peroxidases, in which opaque electronic substance (melanin precursor) is formed, and then the trans-Golgi network produces vesicles containing tyrosinase and dopachrome-rearranging enzymes (Liu & Simon, 2003; Palumbo, 2003). Melanization originate from the precursor matrix and then to form particle-like melanin, which also occurred in *S. pharaonis* (Jiang et al., 2020). However, in this study, the intracellular origins of melanin precursors have not been found in mantle of *C. gigas*, which is a question need to be studied further. Next, most of the melanin granules aggregate in the precursor matrix to form melanosomes, and melanosomes gradually become concentrated in the cytoplasm (Clancy & Simon, 2001; Schraermeyer, 1994). Similarly, the melanocytes from two different developmental stages were observed in *C. gigas* (Figure 6a–c), in this process, melanosomes were further developed and expanded, and their hue gradually increased. Finally, in vertebrates, melanosomes migrate to the cell surface via binding to the cytoskeleton, then fuse with the cell membrane at the apical pole, followed by the melanin granules are discharged into intercellular spaces or lumen by exocytosis or cell fragmentation (Clancy & Simon, 2001; Schraermeyer, 1994). The same thing was also happened in *C. gigas* (Figure 6f). In general, it was established that the possible pathway of melanogenesis in *C. gigas* based on static images, which is similar to the process of the formation of melanin granules in *S. pharaonic* (Jiang et al., 2020) and the process of formation of ommochrome pigment granules in crayfish eyes (Schraermeyer & Stieve, 1991).

5 | CONCLUSION

Taken together, mantle tissue with a dark surface from orange shell color oysters was investigated. Ferrous sulfate staining methods and IF with CgTYR antibody were used to identify the existence of melanin in mantle. Next, melanocytes containing melanosome and other organelles were observed in mantle using TEM, which provided more details about melanosome. Furthermore, elemental distribution of melanosome was analyzed using STEM EDS mapping method for the first time, which was important to better understand the biological properties of melanosome metabolism. In addition, the description of melanogenesis in mantle was clarified based on TEM observation. These data further substantiate the biochemical characters, distribution, and melanogenesis of melanin in mantle of bivalve.

AUTHOR CONTRIBUTIONS

Zhuanzhuan Li: Writing – original draft; data curation. **Qi Li:** Supervision; funding acquisition; conceptualization. **Chengxun Xu:** Resources. **Hong Yu:** Supervision; resources.

ACKNOWLEDGMENTS

The authors are grateful to Jinshan Tan from the State Key Laboratory of Bio-Fibers and Eco-Textiles of Qingdao University for his technical assistance in STEM EDS Mapping analysis. This work was supported by the grants from National Natural Science Foundation of China (31972789), the China Agriculture Research System Project (CARS-49), and the Earmarked Fund for Agriculture Seed Improvement Project of Shandong Province (2020LZGC016, 2021LZGC027).

CONFLICT OF INTEREST

The authors declare that they have no known competing financial interests or personal relationships that could have appeared to influence the work reported in this article.

DATA AVAILABILITY STATEMENT

The data that support the findings of this study are available from the corresponding author upon reasonable request.

ETHICS STATEMENT

The Pacific oyster is neither an endangered nor protected species. All experiments in this study were conducted according to national and institutional guidelines.

ORCID

Qi Li https://orcid.org/0000-0002-3937-9324

REFERENCES

Addadi, L., Joester, D., Nudelman, F., & Weiner, S. (2006). Mollusk shell formation: A source of new concepts for understanding biomineralization processes. *Chemistry-A European Journal*, *12*(4), 980–987. https://doi.org/10.1002/chem.200500980

Biesemeier, A., Eibl, O., Eswara, S., Audinot, J. N., Wirtz, T., Pezzoli, G., Zucca, F. A., Zecca, L., & Schraermeyer, U. (2016). Elemental mapping of neuromelanin organelles of human substantia nigra: Correlative ultrastructural and chemical analysis by analytical transmission electron microscopy and nano-secondary ion mass spectrometry. *Journal of Neurochemistry*, *138*(2), 339–353. https://doi.org/10.1111/jnc.13648

Biesemeier, A., Schraermeyerb, U., & Eibla, O. (2011). Quantitative chemical analysis of ocular melanosomes in stained and non-stained tissues. *Micron*, *42*(5), 461–470. https://doi.org/10.1016/j.micron.2011.01.004

Brake, J., Evans, F., & Langdon, C. (2004). Evidence for genetic control of pigmentation of shell and mantle edge in selected families of Pacific oysters, *Crassostrea Gigas*. *Aquaculture*, *229*(1–4), 89–98. https://doi.org/10.1016/S0044-8486(03)00325-9

Bravo Portela, I., Martinez-Zorzano, V. S., Molist-Perez, I., & Molist García, P. (2012). Ultrastructure and glycoconjugate pattern of the foot epithelium of the abalone *Haliotis tuberculata* (Linnaeus, 1758) (Gastropoda, Haliotidae). *The Scientific World Journal*, *2012*, 960159. https://doi.org/10.1100/2012/960159

Bubel, A. (1973). An electron-microscope investigation of the cells lining the outer surface of the mantle in some marine molluscs. *Marine Biology*, *21*, 245–255. https://doi.org/10.1007/BF003552540

Carriel, V. S., Aneiros-Fernandez, J., Arias-Santiago, S., Garzón, I. J., Alaminos, M., & Campos, A. (2011). A novel histochemical method for a simultaneous staining of melanin and collagen fibers. *Journal of Histochemistry & Cytochemistry*, *59*(3), 270–277. https://doi.org/10.1369/0022155410398001

Clancy, C. M. R., & Simon, J. D. (2001). Ultrastructural organization of eumelanin from Sepia officinalis measured by atomic force microscopy. *Biochemistry*, *40*(44), 13353–13360. https://doi.org/10.1021/bi010786t

Colville, A., & LimA, R. P. (2003). Microscopic structure of the mantle and palps in the freshwater mussels *Velesunio ambiguus* and *Hyridella depressa* (Bivalvia: Hyriidae). *Molluscan Research*, *23*(1), 1–20. https://doi.org/10.1071/MR02014

D'Alba, L., & Shawkey, M. D. (2019). Melanosomes: Biogenesis, properties, and evolution of an ancient organelle. *Physiological Reviews*, *99*(1), 1–19. https://doi.org/10.1152/physrev.00059.2017

Eibl, O., Schultheiss, S., Blitgen-Heinecke, P., & Schraermeyer, U. (2006). Quantitative chemical analysis of ocular melanosomes in the TEM. *Micron*, *37*(3), 262–276. https://doi.org/10.1016/j.micron.2005.08.006

Fang, D. D., Kute, T., & Setaluri, V. (2001). Regulation of tyrosinase-related protein-2 (TYRP2) in human melanocytes: Relationship to growth and morphology. *Pigment Cell Research*, *14*, 132–139. https://doi.org/10.1034/j.1600-0749.2001.140209.x

Feng, D. D., Li, Q., & Yu, H. (2019). RNA interference by ingested dsRNA-expressing bacteria to study shell biosynthesis and pigmentation in *Crassostrea gigas*. *Marine Biotechnology*, *21*, 526–536. https://doi.org/10.1007/s10126-019-09900-2

Han, Y. J., Xie, C. Y., Fan, N. N., Song, H. C., Wang, X. M., Zheng, Y. X., Zhang, M. W., Liu, Y. Q., Huang, B. Y., Wei, L., & Wang, X. T. (2022). Identification of melanin in the mantle of the Pacific oyster *Crassostrea gigas*. *Frontiers in Marine Science*, *9*, 880337. https://doi.org/10.3389/fmars.2022.880337

Hartman, M. L., & Czyz, M. (2015). MITF in melanoma: Mechanisms behind its expression and activity. *Cellular and Molecular Life Science*, *72*, 1249–1260. https://doi.org/10.1007/s00018-014-1791-0

Hong, L., Liu, Y., & Simon, J. D. (2004). Binding of metal ions to melanin and their effects on the aerobic reactivity. *Photochemistry and Photobiology*, *80*(3), 477–481. https://doi.org/10.1562/0031-8655(2004)080<0477:BOMITM>2.0.CO;2

Istin, M., & Masoni, A. (1973). Absorption et redistribution du calcium dans le manteau des lamellibranches en relation avec la structure. *Calcified Tissue Research*, *11*, 151–162. https://doi.org/10.1007/BF02547297

Ito, S., Wakamatsu, K., Glass, K., & Simon, J. D. (2013). High-performance liquid chromatography estimation of cross-linking of dihydroxyindole moiety in eumelanin. *Analytical Biochemistry*, *434*(2), 221–225. https://doi.org/10.1016/j.ab.2012.12.005

Jabbour-Zahab, R., Chagot, D., Blanc, F., & Grizel, H. (1992). Mantle histology, histochemistry and ultrastructure of the pearl oyster *Pinctada margaritifera* (L.). *Aquatic Living Resources*, *5*(4), 287–298. https://doi.org/10.1051/alr:1992027

Jackson, D. J., McDougall, C., Woodcroft, B., Moase, P., Rose, R. A., Kube, M., Reinhardt, R., Rokhsar, D. S., Montagnani, C., Joubert, C., Piquemal, D., & Degnan, B. M. (2010). Parallel evolution of nacre building gene sets in molluscs. *Molecular Biology and Evolution*, *27*(3), 591–608. https://doi.org/10.1093/molbev/msp278

Jiang, M. W., Xue, R. P., Chen, Q., Zhan, P. P., Han, Q. X., Peng, R. B., & Jiang, X. M. (2020). Histology and ultrastructure of ink gland and melanogenesis in the cuttlefish *sepia pharaonic*. *Invertebrate Biology*, *139*, e12306. https://doi.org/10.1111/ivb.12306

Künz, E., & Haszprunar, G. (2001). Comparative ultrastructure of gastropod cephalic tentacles: Patellogastropoda, Neritaemorphi and Vetigastropoda. *Zoologischer Anzeiger – A Journal of Comparative zoology*, *240*, 137–165. https://doi.org/10.1078/0044-5231-00017

Lemer, S., Saulnier, D., Gueguen, Y., & Planes, S. (2015). Identification of genes associated with shell color in the black-lipped pearl oyster. *Pinctada margaritifera*. *BMC Genomics*, *16*, 568. https://doi.org/10.1186/s12864-015-1776-x

Li, Z. Z., Li, Q., Liu, S. K., Han, Z. Q., Kong, L. F., & Yu, H. (2021). Integrated analysis of coding genes and non-coding RNAs associated with shell color in the Pacific oyster (*Crassostrea gigas*). *Marine Biotechnology*, *3*, 417–429. https://doi.org/10.1007/s10126-021-10034-7

Li, Z. Z., Li, Q., Xu, C. X., & Yu, H. (2022). Molecular characterization of *Pax7* and its role in melanin synthesis in *Crassostrea gigas*. *Comparative Biochemistry Physiology Part B: Biochemistry and Molecular Biology*, *260*, 110720. https://doi.org/10.1016/j.cbpb.2022.110720

Liu, Y., & Simon, J. D. (2003). The effect of preparation procedures on the morphology of melanin from the ink sac of Sepia officinalis. *Pigment Cell Research*, *16*(1), 72–80. https://doi.org/10.1034/j.1600-0749.2003.00009.x

Liu, Y., & Simon, J. D. (2005). Metal-ion interactions and the structural organization of sepia eumelanin. *Pigment Cell Research*, *18*(1), 42–48. https://doi.org/10.1111/j.1600-0749.2004.00197.x

Machado, J., Castilho, F., Coimbra, J., Monteiro, E., Sá, C., & Reis, M. (1988). Ultrastructural and cytochemical studies in the mantle of *Anodonta cygnea*. *Tissue and Cell*, *20*(5), 797–807. https://doi.org/10.1016/0040-8166(88)90024-9

Madkhali, N., Alqahtani, H. R., Al-Terary, S., Laref, A., & Haseeb, A. (2019). The doping effect of Fe, Cu and Zn ions on the structural and electrochemical properties and the thermostability of natural melanin extracted from Nigella sativa L. *Journal of Molecular Liquids.*, *285*, 436–443. https://doi.org/10.1016/j.molliq.2019.04.063

Martin, G. G., Stamnes, S., Henderson, N., Lum, J., Rubin, N., & Williams, J. P. (2021). Hemocyte activation and nodule formation in the giant keyhole limpet, *Megathura crenulata*. *Invertebrate Biology*, *137*(2), 151–170. https://doi.org/10.1111/ivb.12213

McDougall, C., Green, K., Jackson, D. J., & Degnan, B. M. (2011). Ultrastructure of the mantle of the gastropod Haliotis asinina and mechanisms of shell regionalization. *Cells, Tissues, Organs*, *194*(2–4), 103–107. https://doi.org/10.1159/000324213

Min, Y., Li, Q., & Yu, H. (2022). Heme-peroxidase 2 modulated by POU2F1 and SOXS is involved in pigmentation in Pacific oyster (*Crassostrea gigas*). *Marine Biotechnology*, *24*, 263–275. https://doi.org/10.1007/sl0126-022-10098-z

Nogal, R. Á., & García, P. M. (2015). The outer mantle epithelium of *Haliotis tuberculate* (Gastropoda Haliotidae): An ultrastructural and histochemical study using lectins. *Acta Zoologica*, *96*(4), 452–459. https://doi.org/10.1111/azo.12090

Ordóñez, N. G. (2014). Value of melanocytic-associated immunohistochemical markers in the diagnosis of malignant melanoma: A review and update. *Human Pathology*, *45*(2), 191–205. https://doi.org/10.1016/j.humpath.2013.02.007

Palumbo, A. (2003). Melanogenesis in the ink gland of Sepia officinalis. *Pigment Cell Research*, *16*, 517–522. https://doi.org/10.1034/j.1600-0749.2003.00080.x

Prince, J. S., & Young, D. (2010). Ultrastructural study of skin coloration in *Aplysia Californica*. *Bulletin of Marine Science*, *86*(4), 803–812. https://doi.org/10.5343/bms.2009.1075

Ruska, A. B., Alfaro, A. C., Young, T., Watts, E., & Adams, S. L. (2020). Development stage of cryopreserved mussel (*Perna canaliculus*) larvae influences post-thaw impact on shell formation, organogenesis, neurogenesis, feeding ability and survival. *Cryobiology*, *93*, 121–132. https://doi.org/10.1016/j.cryobiol.2020.01.021

Saenko, S. V., & Schilthuizen, M. (2021). Evo-devo of shell colour in gastropods and bivalves. *Current Opinion in Genetic & Development*, *69*, 1–5. https://doi.org/10.1016/j.gde.2020.11.009

Saliba, E., & Bhawan, J. (2021). Aberrant expression of immunohistochemical markers in malignant melanoma: A review. *Dermatopathology*, *8*(3), 359–370. https://doi.org/10.3390/dermatopathology8030040

Sarzanini, C., Mentasti, E., Abollino, O., Fasano, M., & Aime, S. (1992). Metal-ion content in Sepia officinalis melanin. *Marine Chemistry*, *39*(4), 243–250. https://doi.org/10.1016/0304-4203(92)90011-X

Schraermeyer, U. (1994). Fine structure of melanogenesis in the ink sac of *Sepia officinalis*. *Pigment Cell Research*, *7*(1), 52–60. https://doi.org/10.1111/j.1600-0749.1994.tb00018.x

Schraermeyer, U., & Stieve, H. (1991). Peroxidase and tyrosinase are present in secondary lysosomes that degrade photosensory membranes

of the crayfish photoreceptor: Possible role in pigment granule formation. *Pigment Cell Research*, *4*(4), 163–171. https://doi.org/10.1111/j.1600-0749.1991.tb00434.x

Shataer, M., Shataer, S., Liao, L. B., Li, T., & Bai, S. B. (2020). Histological comparison of two special methods of staining melanin in human skin. *International Journal of Morphology*, *38*(6), 1535–1538. https://doi.org/10.4067/S0717-95022020000601535

Wang, Y., Wang, C. L., Zhan, P. P., & Song, W. W. (2011). Histological and ultrastructural observation of the ink sac of Octopus variabilis. *Journal of Fisheries*, *35*, 1633–1639 (in Chinese with English abstract).

Xu, X., Chu, A. Y., Pasha, T. L., Elder, D. E., & Zhang, P. J. (2002). Immunoprofile of MITF, tyrosinase, melan-a, and MAGE-1 in HMB45-negative melanomas. *The American Journal of Surgical Pathology*, *26*(1), 82–87. https://doi.org/10.1097/00000478-200201000-00010

Yu, F. F., Pan, Z. N., Qu, B. L., Yu, X. Y., Xu, K. H., Deng, Y. W., & Liang, F. L. (2018). Identification of a tyrosinase gene and its functional analysis in melanin synthesis of *Pteria penguin*. *Gene*, *656*, 1–8. https://doi.org/10.1016/j.gene.2018.02.060

Yu, F. F., Qu, B. L., Lin, D. D., Deng, Y. W., Huang, R. L., & Zhong, Z. M. (2018). Pax3 gene regulated melanin synthesis by tyrosinase pathway in *Pteria penguin*. *International Journal of Molecular Science*, *19*, 3700. https://doi.org/10.3390/ijms19123700

Żądło, A. C., & Sarna, T. (2019). Interaction of iron ions with melanin. *Acta Biochimica Polonica*, *66*(4), 459–462. https://doi.org/10.18388/abp.2019_2889

Zhang, B., Zhang, D. G., Ye, D. Y., Hong, C. Z., & Yang, L. J. (2020). Comparison of ferrous sulfate method and Fontana method for melanin display. *Journal of Shantou University Medical College*, *33*(1), 46–48 (in Chinese with English abstract).

Zhang, S. J., Wang, H. X., Yu, J. J., Jiang, F. J., Yue, X., & Liu, B. Z. (2018). Identification of a gene encoding microphthalmia-associated transcription factor and its association with shell color in the clam Meretrix petechialis. *Comparative Biochemistry Physiology Part B: Biochemistry and Molecular Biology*, *225*, 75–83. https://doi.org/10.1016/j.cbpb.2018.04.007

Zhu, Y. J., Li, Q., Yu, H., Liu, S. K., & Kong, L. F. (2021). Shell biosynthesis and pigmentation as revealed by the expression of tyrosinase and tyrosinase-like protein genes in Pacific oyster (*Crassostrea gigas*) with different shell colors. *Marine Biotechnology*, *23*, 777–789. https://doi.org/10.1007/s10126-021-10063-2

SUPPORTING INFORMATION

Additional supporting information can be found online in the Supporting Information section at the end of this article.

How to cite this article: Li, Z., Li, Q., Xu, C., & Yu, H. (2022). Histological, elemental, and ultrastructural analysis of melanin in mantle of Pacific oyster (*Crassostrea gigas*). *Microscopy Research and Technique*, 1–11. https://doi.org/10.1002/jemt.24269